Effect of Surfactant on the Drying Patterns of Graphite Nanofluid Droplets

ARTICLE *in* THE JOURNAL OF PHYSICAL CHEMISTRY B · MAY 2013

Impact Factor: 3.3 · DOI: 10.1021/jp401751z · Source: PubMed

2 AUTHORS, INCLUDING:

Alexandru Crivoi

Nanyang Technological University

19 PUBLICATIONS **165** CITATIONS

SEE PROFILE

THE JOURNAL OF PHYSICAL CHEMISTRY B

Article

pubs.acs.org/JPCB

Effect of Surfactant on the Drying Patterns of Graphite Nanofluid Droplets

Alexandru Crivoi and Fei Duan*

School of Mechanical and Aerospace Engineering, Nanyang Technological University, Singapore 639798

Supporting Information

ABSTRACT: We investigate the effect of surfactant on the formation of nanoparticle aggregates that resulted from evaporation of sessile nanofluid droplets theoretically and experimentally. A Monte Carlo model is developed to explain the transition from the coffee-ring pattern to the uniform deposition in drying the pinned sessile nanofluid droplets. The model applies the diffusion limited cluster−cluster aggregation approach coupled with the biased random walk of nanoparticles. The experiments show that the addition of surfactant in nanofluids helps the formation of a coffee ring instead of the uniform domain coverage. The simulations suggest an explanation of this transition by controlling the sticking probability parameter between the particles. The simulated results statistically agree with the experimental observation of the finally dried graphite nanoparticle structures from the pinned nanofluid droplets.

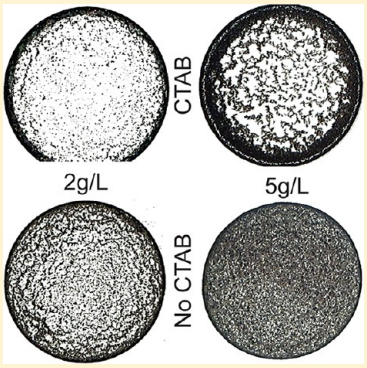

INTRODUCTION

After nanofluid solvent evaporation, the remaining particles can form various complex self-assemblies on the substrate.[1−6] The coffee-ring pattern[7,8] was commonly observed after full drying of the pinned colloidal droplets,[9−11] while the other structures, such as dual-scale structures,[12] networks,[13] worm-like and ribbon-like islands,[14,15] fractal cavities[16] and particle aggregates,[17] fingering instabilities,[18,19] and stalagmites,[20] were reported in the experiments with the thin-film drying. More sophisticated multicomponent structures also appeared in dried blood spots[21] and protein samples.[22] Despite a significant number of the reported experimental results, the controlled deposition of particles by using colloidal droplet evaporation is still a challenge. Several interesting approaches to model the particle deposition during the colloid drying were also developed for the observed phenomena.[17,23−26] Recently, Yunker et al. achieved an interesting transition from the coffee-ring effect to the uniform deposition by changing the shape of polystyrene microparticles.[10] In the present work, another way to alter the deposition pattern by influencing the long-range particle interaction is explored. Experimental results are supported by the simulation study, which aims to uncover both the structure evolution process with time and trends in pattern morphology changes under different controlled conditions.

EXPERIMENTAL METHOD

In the experiments, the suspensions of 2−3 nm graphite nanoparticles (Sky Spring Nanomaterials Inc.) in the deionized water were prepared into the 2 and 5 g/L nanofluid in mass concentration. Cetyltrimethylammonium bromide (CTAB) surfactant was added into half of the prepared samples. A total of four nanofluid samples were used: containing 2 or 5 g/L graphite particles, without the surfactant or with the surfactant at 0.1% concentration in weight. As a cationic dispersant, CTAB can keep particles well dispersed in the base fluids.[27,28] Therefore, the addition of surfactant in the nanofluid is associated with the decreased particle sticking probability, and the nanofluids free of surfactant are considered to have a higher sticking probability. The nanoparticle sample preparation is carried out by using a sensitive mass balance with an accuracy of 0.1 mg. The mixed nanofluids were well stirred first, and then kept in an ultrasonication bath (Fisher Scientific model 500) for more than 2 h to ensure the even dispersion of the nanoparticles in the base fluids initially. The detailed nanofluid preparation process was described.[27,29] The silicon wafer was used as a substrate for the nanofluid droplet drying. In order to prevent the following agglomeration with time, right after the suspensions were prepared, a tiny sessile droplet with 1 mm or less in diameter was placed on a clean substrate to dry naturally, as shown in the inset of Figure 1. The drying is in the open conditions of 25 °C in temperature, 1 atm in pressure, and 40% in relative humidity. The drying patterns were directly recorded with the optical microscope (Zeiss Axioscop II) and further processed with Matlab for statistical calculations. The phase separation between surfactant and graphite nanoparticles was not observed on the surface of nanofluid droplets for 0.1% concentration of CTAB. The phase separation might happen with significantly higher CTAB concentrations (1% for example). The experimental observation suggests that the observed coffee-ring formation at 0.1% is caused by the changes in particle interactions.

Received: February 19, 2013
Revised: April 9, 2013
Published: April 17, 2013

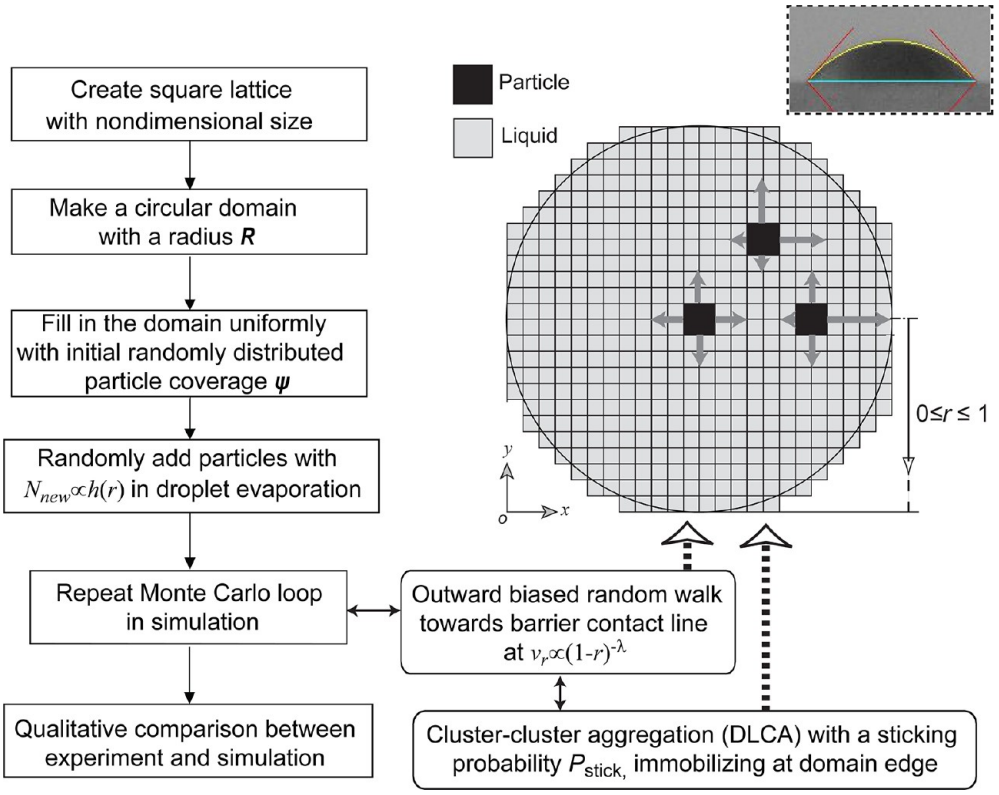

Figure 1. The schematic representation of the capillary flow implementation. The circular domain with the square lattice inside is filled with liquid with the randomly distributed particles. Particles (2 × 2 cells) are allowed to randomly move inside liquid, but the probability distribution promotes the motion in the outward radial direction in Monte Carlo simulation.

MODEL

A mathematical model is developed from the diffusion limited cluster−cluster aggregation (DLCA) process[30] by implementing the concept of the biased random walk (BRW) of particles on a two-dimensional (2D) lattice in a circular domain.[31] The domain shape in Figure 1 is the top view of the pinned sessile droplets, shown in the inset. As shown in Figure 1, the circular domain is assigned with a diameter, which varies from 150 to 1000 cells in the study. Note that the nonsmooth edge can be neglected if the cell number is large enough. To show the significant effect of the long-ranged interparticle interaction, the particles are assumed having the same size at 2 × 2 cells but the different sticking probabilities in the different simulation. On each step of the simulation, each single particle performs a random move within the circular domain, with a probability distribution, $p_{move} = \{l(x, y), r(x, y), u(x,y), d(x,y)\}$, for the (left, right, up, down) directions on a 2D lattice. Before the particles reach the contact line of the circular domain, the general BRW on the 2D lattice follows the probabilities defined as p_{move}, which also obey the no-waiting condition at $u(x, y) + d(x, y) + l(x, y) + r(x, y) = 100\%$ and the symmetric condition at $u(x, y) + d(x, y) = 50\%$. Then, a corresponding form of the governing Fokker−Planck equation for the probability density function (PDF) can be deducted[32]

$$\frac{\partial p(x, y)}{\partial t} = -\frac{\partial}{\partial x}(v_x(x, y)p(x, y)) - \frac{\partial}{\partial y}(v_y(x, y)p(x, y)) + D\left(\frac{\partial^2 p(x, y)}{\partial x^2} + \frac{\partial^2 p(x, y)}{\partial y^2}\right) \quad (1)$$

where $p(x, y)$ is the probability density, $v_x(x, y)$ and $v_y(x, y)$ are the horizontal and vertical drift rates derived from p_{move},[32] and D is the diffusion coefficient. Since it was assumed that the random walker always makes a move in either the horizontal or vertical direction with equal probabilities, D is constant. Equation 1 is used to model the particle migration inside the drying pinned sessile droplet. It is assumed that the diffusion process associated with Brownian motion is coupled with the capillary transport of particles toward the pinned contact line of the droplet. The resultant drift rate v_r with a value of $(v_x^2(x, y) + v_y^2(x, y))^{1/2}$ represents the capillary flow velocity, which, according to Deegan et al.,[7] obeys the relation $v_r \propto (1 - r)^{-\lambda}$, where $0 \le r \le 1$ is the scaled droplet radius and $\lambda = (\pi - 2\theta)/(2\pi - 2\theta)$, where θ is the droplet contact angle. Physically, increasing velocity toward the edge of the droplet might be induced by the uneven evaporation flux with the highest value at the contact line of the droplet.[9,33−36]

Adjusting the conditions with keeping continuity at the center $r = 0$ and eliminating the singularity at the contact line $r = 1$, we can derive the probability distribution, used in the Monte Carlo simulation:

$$\left\{\begin{aligned} r(x, y) &= x\frac{(1 - |x| + \varepsilon)^{-\lambda}}{4\varepsilon^{-\lambda}} + \frac{1}{4} \\ l(x, y) &= -x\frac{(1 - |x| + \varepsilon)^{-\lambda}}{4\varepsilon^{-\lambda}} + \frac{1}{4} \\ u(x, y) &= y\frac{(1 - |y| + \varepsilon)^{-\lambda}}{4\varepsilon^{-\lambda}} + \frac{1}{4} \\ d(x, y) &= -y\frac{(1 - |y| + \varepsilon)^{-\lambda}}{4\varepsilon^{-\lambda}} + \frac{1}{4} \end{aligned}\right\} \quad (2)$$

dx.doi.org/10.1021/jp401751z | J. Phys. Chem. B 2013, 117, 5932−5938

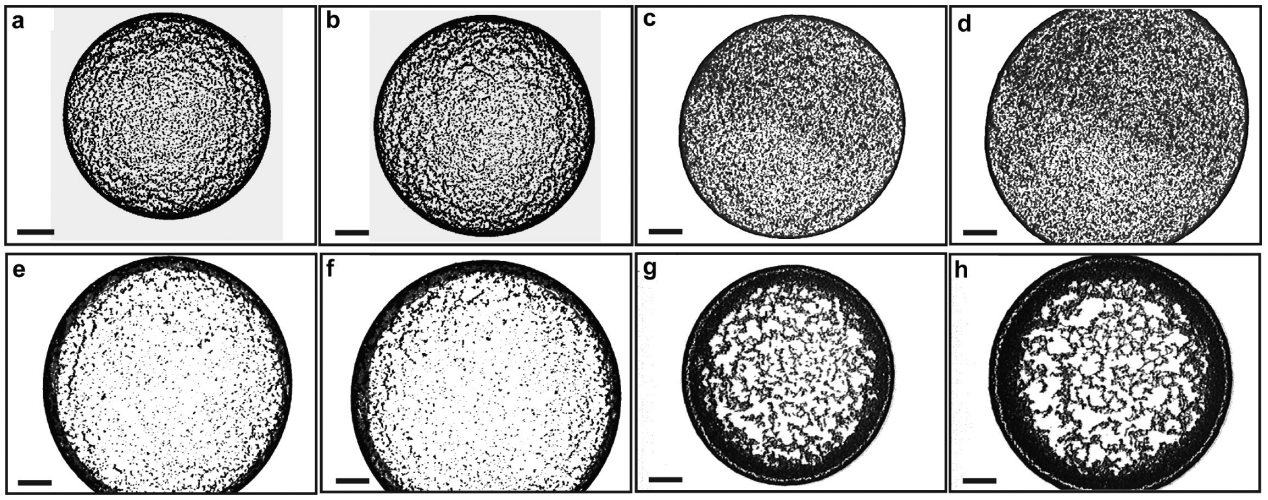

Figure 2. The experimental images of dried water-based nanofluid droplets. (a–d) No surfactant was added, and the mass concentration of 2–3 nm graphite nanoparticles is at (a, b) 2 g/L and (c, d) 5 g/L. (e–h) The CTAB surfactant at 0.1 wt % was added, and the mass concentration of 2–3 nm graphite nanoparticles is at 2 g/L (e, f) and 5 g/L (g, h).

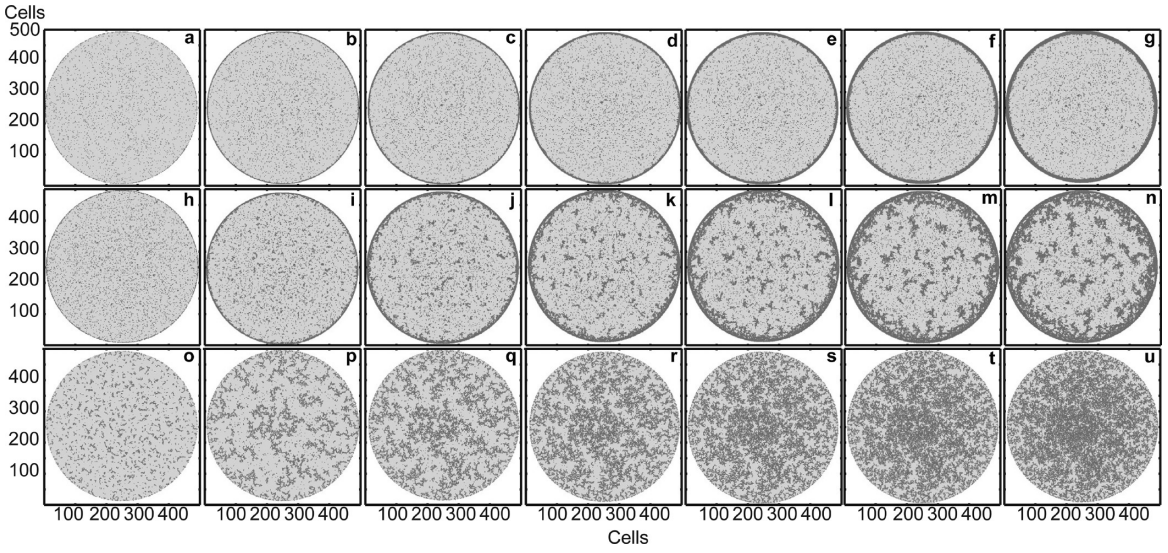

Figure 3. The progress of DLCA simulations in time. The circular domain diameter is 500 cells, the sticking probability values are 0.1% (a–g), 0.5% (h–n), and 25% (o–u), and the initial particle coverage is 5% (a–g) and 10% (h–u). The images in each row are captured continuously from 100 to 2500 MCS with a step of 400 MCS.

where $-1 \leq x \leq 1$ and $-1 \leq y \leq 1$ are the scaled Cartesian particle coordinates.

The Monte Carlo simulation of the capillary particle transport is started by initially placing a number of particles at random positions on the 2D lattice inside the circular domain, shown in Figure 1. Each particle is treated as a random walker, making one move in a Monte Carlo step (MCS) following eq 2. As the simulation progresses, new particles are continuously placed inside the domain according to the rule $N_{new} \propto h(r)$, in which $h(r)$ is the thickness profile of an assumed spherical cap, with $((1/\sin\theta)^2 - r^2)^{1/2} - 1/\tan\theta$. It is used to recall that more particles start the outward motion from the thicker part of the droplet as the height of the pinned droplet shrinks with evaporation. Therefore, every 10 MCS, we randomly place $N_{new}(r)$ additional particles inside the domain. The number of new particles placed is also proportional to the initial particle coverage ψ.

The value of p_{stick} is fixed throughout each of the simulation runs. If any particles aggregate into a cluster, on the next MCS, the cluster is treated similarly to other single particles and performs random moves with the same value of p_{move}. It means that all the particles which compose the cluster move in one sampled direction simultaneously. However, the individual particle and large cluster diffusivities are actually not the same, since the implemented exclusion principle states that two different particles are not allowed to occupy the same lattice position at once. This restriction forces large clusters to skip a larger number of moves, since their boundaries are larger than those of single particles or small clusters. Longer average waiting times in the BRW model result in lower diffusivity.[31] The cluster coordinates, $\langle x \rangle$ and $\langle y \rangle$, are averaged for the correspondent coordinates of the contained particles. All the clusters are allowed to progressively stick to each other with the same probability p_{stick} and form larger aggregates. The simulation runs are performed on a nondimensional 500 × 500 or 1000 × 1000 lattice, and hence do not include as many particles as are present in the real experiments. However, the present simulation of 2D particle

dx.doi.org/10.1021/jp401751z | J. Phys. Chem. B 2013, 117, 5932–5938

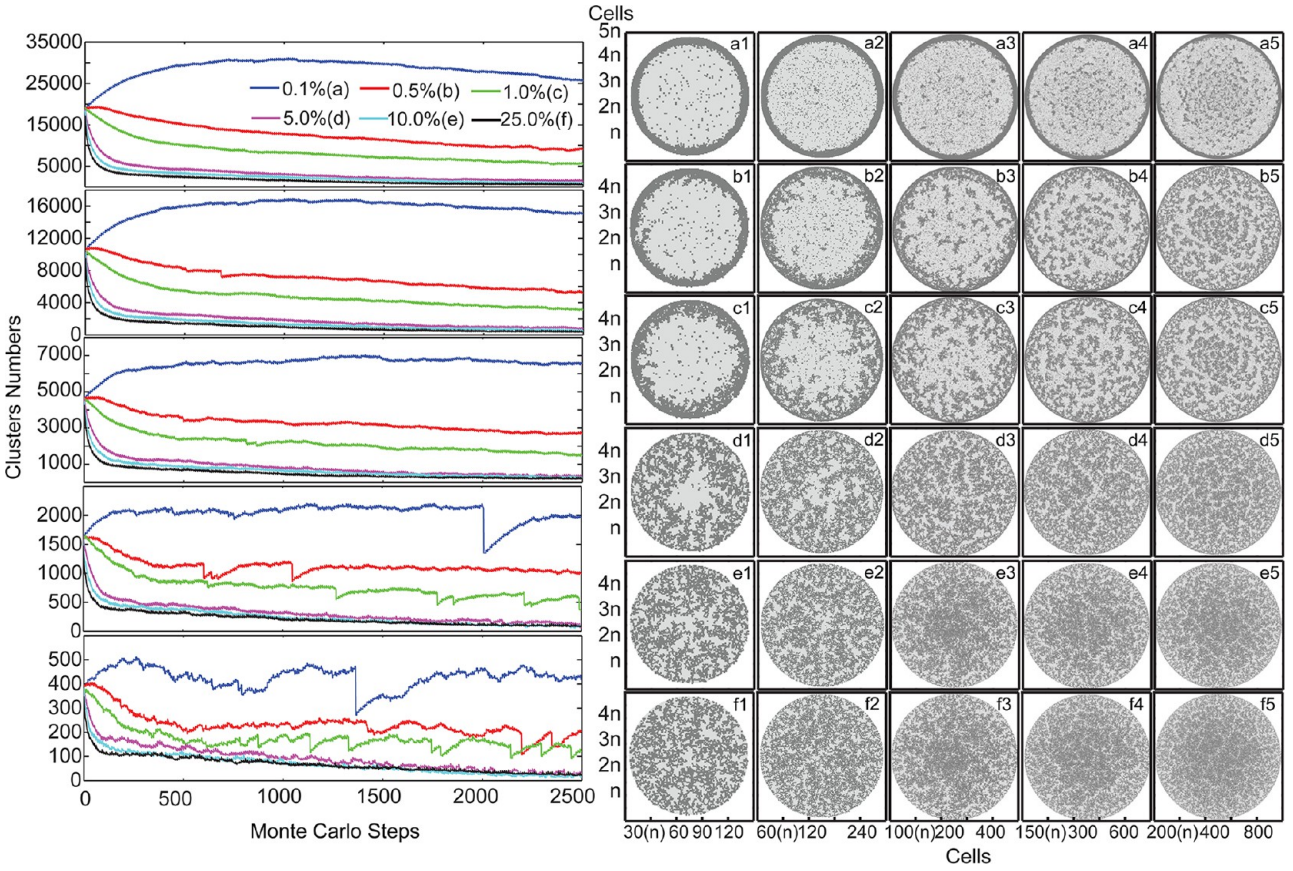

Figure 4. The DLCA results for 10% initial particle coverage are shown on the right side. The sticking probability values are varied at (a) 0.1%, (b) 0.5%, (c) 1%, (d) 5%, (e) 10%, and (f) 25%. The circular domain diameter is varied at (1) 150, (2) 300, (3) 500, (4) 750, and (5) 1000 cells. All results are shown after 2500 MCS. The progression of total cluster number during the simulation runs is shown on the left side. The domain size values are changed from top to bottom at 1000, 750, 500, 300, and 150 cells for the corresponding diagrams.

transport inside the drying droplet shows several characteristic trends which are recalled in the present experiments.

RESULTS AND DISCUSSION

In the experiments, using the high-concentration 5 g/L graphite nanofluids without CTAB surfactant leads to the uniform-like coverage of the dried spots (see Figure 2c,d), while the dilute 2 g/L solution leads to the transient, mixed pattern. Figure 2a,b shows the concentric particle front-lines, resulting from the jammed outward flow and having higher particle density than the droplet center.

The addition of surfactant to the dilute (2 g/L) solution of graphite particles leads to the classical coffee-ring effect, as shown in Figure 2e,f. Most of the particles accumulate near the edge of the spot, while the inner surface is left almost free of particles; the results are similar to the investigation of Deegan et al.[7] A more interesting complicated pattern is observed for the graphite particles at the 5g/L nanofluids with the CTAB surfactant added (Figure 2g,h). Two structures coexist in the final state: a thick and relatively loosely packed coffee ring (small gaps can be noted between the particles in the coffee ring) is filled inside with a sparse network of cluster aggregates.

The simulation results describe step by step the formation of a coffee ring (Figure 3a–g), mixed pattern (Figure 3h–n), and uniform coverage (Figure 3o–u). Figure 3a–g illustrates that the coffee-ring thickness is gradually increased during the whole simulation run with p_{stick} = 0.1%. Also, no large clusters appear inside the ring even at last steps (see Figure 3g). The results are different if the sticking probability is slightly increased to 0.5%. As seen from Figure 3h–n, some aggregation is evident in the bulk of the liquid even at early stages (Figure 3j). Later, those clusters which are closer to the edge of the circular domain reach the coffee ring and compose its second, more loosely packed and thicker layer. Other clusters which are located close to the domain center accumulate more particles during the latest stages and remain distanced from the coffee ring in the final state (Figure 3n). Therefore, we obtain a mixed particle structure for p_{stick} = 0.5%: a main coffee ring at the edge and secondary clusters inside the ring. The model behavior dramatically changes at p_{stick} = 25%. At the very early stages, all the particles throughout the domain start to aggregate into branched structures (Figure 3o,p). These structures continue to progressively aggregate with each other, and one large structure is rapidly formed, spreading over the whole domain and containing all the previously formed clusters (Figure 3r). Newly added particles slowly fill in the gaps between the branches, and the overall particle distribution becomes more uniform as a function of time (Figure 3s–u).

The final result dependence on both the lattice size and sticking probability is illustrated in (Figure 4). Even for the smallest sticking probability value at 0.1%, the emergence of noticeable particle lumps is evident inside the largest domain (Figure 4 (a5)), while the small domains do not contain any aggregates except the coffee ring (Figure 4 (a1, a2)). This fact can be explained by the observation that for a larger domain diameter most of the particles have a longer path to drift until they reach the boundary ring. A longer drifting path results in more

dx.doi.org/10.1021/jp401751z | J. Phys. Chem. B 2013, 117, 5932–5938

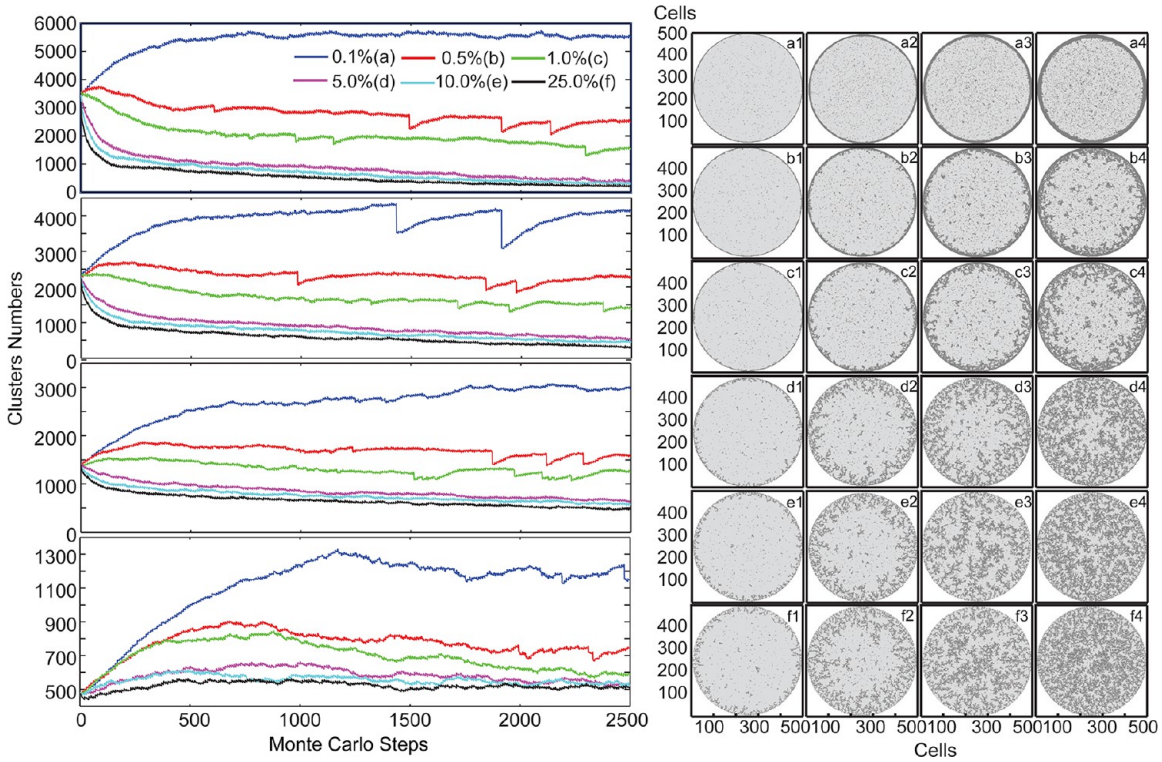

Figure 5. The DLCA results for 500 × 500 domain size. The sticking probability values are at 0.1% (a), 0.5% (b), 1% (c), 5% (d), 10% (e), and 25% (f). The initial particle coverage (ψ) changes at (1) 1%, (2) 3%, (3) 5%, and (4) 7.5%. The progression of total cluster number during the simulation runs is shown on the left side. All the results are shown after 2500 MCS. The initial particle coverage is reduced from top to bottom for the corresponding diagrams, and the sticking probability values correspond to the different curves.

collisions with the neighbor particles in the way, and even for a rather low sticking chance a few aggregation events inevitably occur. Moreover, the growth of small clusters provokes more collisions and even more aggregation events happen, thus leading to even larger lumps. As the aggregation intensifies, the clusters consequently snowball; however, they do not get a branched structure, since a low p_{stick} value causes a low fractal dimension of DLA clusters but with dense and lumpy structures. Increasing p_{stick} to 5% results in the formation of fine uniform coverage on a large lattice (Figure 4 (d5)), while there is still a center gap on the smallest lattice (Figure 4 (d1)). On the largest lattice for the maximal used value of p_{stick} = 25%, the particle coverage becomes denser near the center (Figure 4 (f5)).

The dynamics of the total cluster number is illustrated in the curves of Figure 4. Some sharp drops in the total cluster number can be noticed (especially for the small lattice size). These sharp drops indicate big aggregation events and are specific for coffee-ring formation. In the case of a large number of particles or small clusters accumulated near the edge, adjacent to each other, they do not aggregate yet due to the low sticking probability. Afterward, at some certain time moment, all the particles aggregate into a single coffee ring and cause a sharp decline in cluster number on a single MCS. The drop points to a coffee-ring existence; however, the opposite is not always true. The coffee ring can also grow, adding a smaller number of particles on each MCS. For example, Figure 4 shows that 0.1% sticking on the smallest lattice with a diameter of 150 cells does not result in significant changes, while the simulation on a larger lattice with a diameter of 300 cells experiences the largest, almost 50% drop in total cluster count prior to the end of the run. It is especially noticeable for larger lattices when particles require more time to reach the domain boundary.

The parameter study is completed with the investigation of model behavior on a fixed-size, 500 × 500 lattice with varied p_{stick} and initial particle coverage (Figure 5). All the statistical dependencies of the total cluster number dynamics are provided on the left side of Figure 5 as well. The results show that both the particle coverage and sticking probability parameters are essential in shaping the final structures. Note that if the initial particle coverage is 3% or below (Figure 5 (a1, b1, c1, d1, e1, f1, a2, b2, c2, d2, e2, f2)), the uniform distribution cannot be reached even for high p_{stick} (Figure 5 (f1, f2)). When the coverage reaches 5%, the particles become distributed quite evenly for p_{stick} above 5% (Figure 5 (e3, f3)). Further rising of particle count provides an even better uniformity (Figure 5 (f4)). The interesting statistics are provided in the curves of Figure 5. The total number of clusters grows in the beginning of all the simulation runs with 1% initial coverage. It means that particles are rare at the initial time moment that even a high sticking chance does not cause many aggregation events. After some time (around 500 MCS in most cases), the cluster number stabilizes and even starts to slip in further run. The results for 7.5% coverage are significantly different: the trend highly depends on the p_{stick} value. Only the smallest value with p_{stick} = 0.1% leads to an initial cluster number growth until it reaches some certain saturation value and keeps stable around it. A slightly higher value of p_{stick} = 0.5% results in a very short-term increase in cluster number, followed by slow descending. The other simulation runs with 7.5% initial coverage and a higher p_{stick} experience an immediate fall in cluster numbers. The behavior indicates that no coffee ring can be formed as a result, since the cluster aggregation intensity is too high.

We perform a statistical comparison of the final particle distribution between the simulation results and the experimental

dx.doi.org/10.1021/jp401751z | J. Phys. Chem. B 2013, 117, 5932−5938

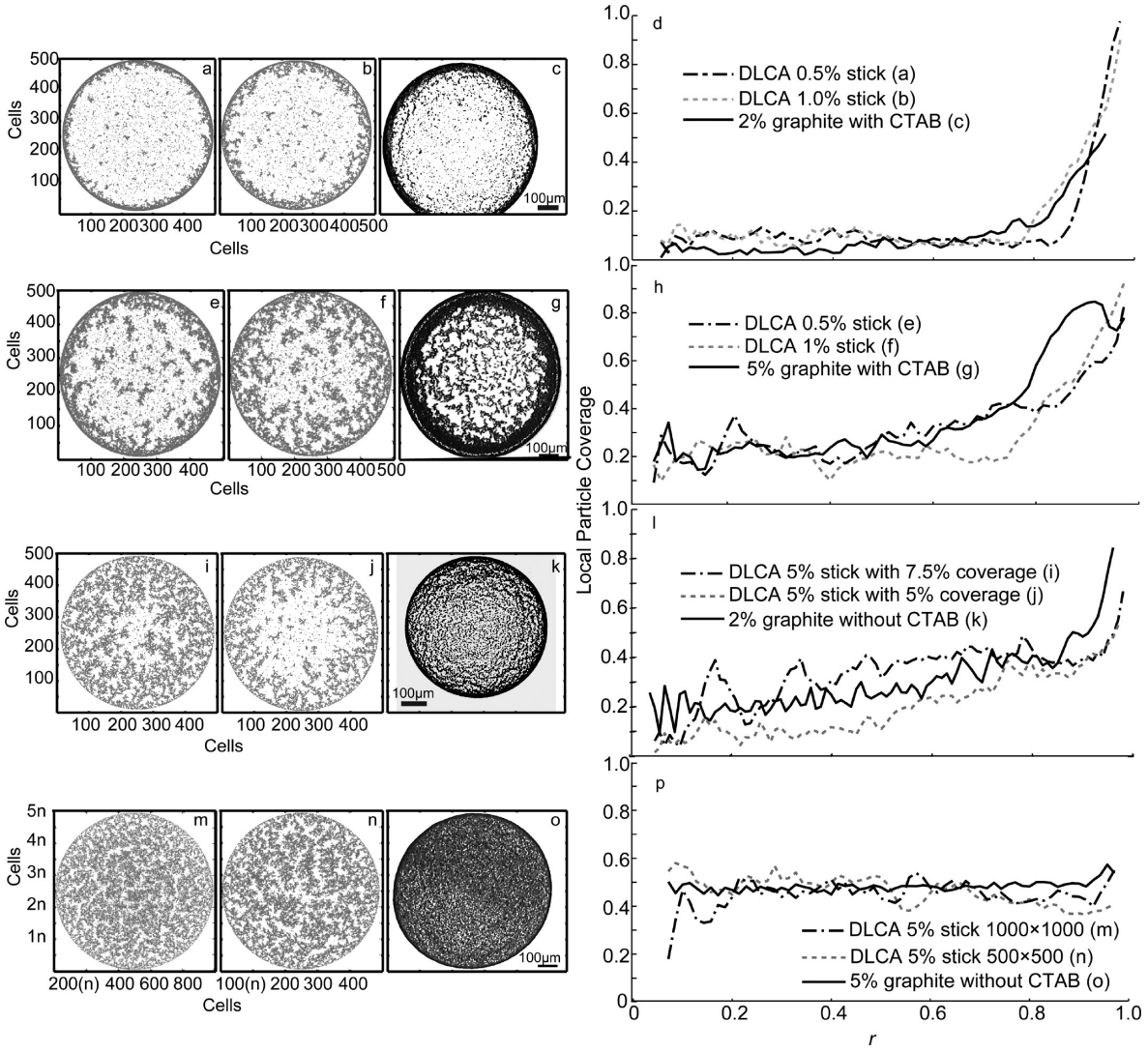

Figure 6. Comparison of the experiments and simulation. The coffee rings display the particle distribution profiles in the simulated patterns (a, b), captured after 2500 MCS with the initial particle coverage at 5%, and the finally dried experimental graphite structure from 2% graphite nanofluid with CTAB (c); the local particle comparison for coffee rings is in part d. The mixed patterns display the particle distribution profiles in the simulated patterns (e, f), captured after 2500 MCS and the initial particle coverage at 10%, and the finally dried experimental graphite structure from 5% graphite nanofluid with CTAB (g); the local particle comparison for mixed patterns with surfactant is in part h. The transient deposition patterns display the particle distribution profiles in the simulated patterns (i, j), captured after 2500 MCS and the initial particle coverage at 10%, and the finally dried experimental graphite structure 2% graphite nanofluid without CTAB (k); the local particle comparison for mixed patterns without surfactant is in part l. The simulation results captured after 2500 MCS with 10% initial coverage (m, n), the finally dried experimental structure of 5% graphite nanofluids (o), and the comparison of the simulated and experimental results with the uniform-like coverage (p).

graphite structures from the dried sessile nanofluid droplets, as shown in Figure 6. From the experimental and simulation images, we estimate the local coverage within the range from 0 to 1 at the varied distance from the domain center. For this purpose, the circular domain is split into 70 concentric rings or "layers", and the average coverage is calculated within each of the layers. The summarized plots show that the particle coverage sharply rises closer to the domain edge for the coffee-ring patterns (Figure 6d), smoothly rises for the mixed patterns (Figure 6h,l), and oscillates within a narrow range of values for the uniform patterns (Figure 6p).

In all, the statistical comparison shows a good agreement between the experimental and simulated patterns. The investigation reveals that the addition of surfactant is associated with the promotion of the coffee-ring deposition of graphite nanoparticles, as well as the low sticking of simulated particles (see Figure 6a–d and Figure 6e–h). A higher concentration of particles sophisticates the coffee-ring patterns, and the effect is well reproduced in the simulations (Figure 6i–l). The results of experiments without surfactant correspond to the simulations with higher sticking probabilities p_{stick} = 5%, and also exhibit a similar dependence on the particle coverage (see Figure 6i–l and Figure 6m–p). A high concentration of graphite particles without surfactant produces a fine uniform coverage, as well as the simulations with a higher particle coverage and a higher sticking probability (Figure 6m–p). Lowering the particle numbers in both the experiments and simulations causes a similar response in the results, producing the transient structures (Figure 6i–k). The particle count is not big enough to cover the domain uniformly, and the local coverage rises toward the edge of the domain but not as sharp as in the case of the classical coffee ring (Figure 6a–c). It is interesting that the density profiles of the

dx.doi.org/10.1021/jp401751z | J. Phys. Chem. B 2013, 117, 5932–5938

two transient structures shown in Figure 6e−g and Figure 6i−k are slightly similar, despite the significant difference in the parameters (the particle concentration and the usage of surfactant) and the visible qualitative difference. However, the trend for the second mixed pattern, shown in Figure 6i−l, is smoother and rather close to the uniform coverage, while another pattern is still closer to the coffee ring in Figure 6e−h. On the basis of this comparison, the addition of surfactant and the associated change in particle interaction is a crucial parameter controlling the transition from uniform deposition to coffee ring, while the other parameters, such as particle concentration and spot size, are also important in shaping the final morphology.

CONCLUSIONS

The experimental results show that the addition of surfactant into a nanofluid can be used to control the final nanoparticle deposition pattern after the full evaporation of the base fluid, deionized water in the graphite nanofluid droplets. The DLCA-based mathematical model has been used to explain the experimentally observed difference by assuming the different interparticle sticking probability in the different nanofluids. In this case, the high sticking probability values are assigned to the particles with no surfactant. The simulated and experimental results demonstrate a statistical agreement in both the final deposition results and the observed response to changes in the controlled parameters. The presented simulation approach explains the variety of the observed structures and can also be used further to investigate more advanced ways to control the particle deposition patterns.

ASSOCIATED CONTENT

Supporting Information

The animations of the coffee ring (jp401751z_si_001.mpg), mixed patterns [low coverage (jp401751z_si_003.mpg) and high coverage (jp401751z_si_002.mpg)], and uniform deposition (jp401751z_si_004.mpg) are provided. This material is available free of charge via the Internet at http://pubs.acs.org.

AUTHOR INFORMATION

Corresponding Author

*E-mail: feiduan@ntu.edu.sg. Phone: +65 67905510. Fax: +65 67924062.

Notes

The authors declare no competing financial interest.

ACKNOWLEDGMENTS

The authors acknowledge the support of A*Star Public Sector Funding (1121202010). The authors also acknowledge the essential help from the NTU student, Mr. John Tan, in conducting the experimental work.

REFERENCES

(1) Yosef, G.; Rabani, E. *J. Phys. Chem. B* **2006**, *110*, 20965−20972.
(2) Murray, C. B.; Kagan, C. R.; Bawendi, M. G. *Science* **1995**, *270*, 1335−1338.
(3) Freeman, R. G.; Grabar, K. C.; Allison, K. J.; Bright, R. M.; Davis, J. A.; Guthrie, A. P.; Hommer, M. B.; Jackson, M. A.; Smith, P. C.; Walter, D. G.; Natan, M. J. *Science* **1995**, *267*, 1629−1632.
(4) Andres, R. P.; Bielefeld, J. D.; Henderson, J. I.; Janes, D. B.; Kolagunta, V. R.; Kubiak, C. P.; Mahoney, W. J.; Osifchin, R. G. *Science* **1996**, *273*, 1690−1693.
(5) Kuncicky, D. M.; Bose, K.; Costa, K. D.; Velev, O. D. *Chem. Mater.* **2007**, *19*, 141−143.
(6) Warner, M. R. E.; Craster, R. V.; Matar, O. K. *J. Colloid Interface Sci.* **2003**, *267*, 92−110.
(7) Deegan, R. D.; Bakajin, O.; Dupont, T. F.; Huber, G.; Nagel, S. R.; Witten, T. A. *Nature* **1997**, *389*, 827−829.
(8) Bigioni, T. P.; Lin, X.-M.; Nguyen, T. T.; Corwin, E. I.; Witten, T. A.; Jaeger, H. M. *Nat. Mater.* **2006**, *5*, 265−270.
(9) Deegan, R. D.; Bakajin, O.; Dupont, T. F.; Huber, G.; Nagel, S. R.; Witten, T. A. *Phys. Rev. E* **2000**, *62*, 756−765.
(10) Yunker, P. J.; Still, T.; Lohr, M. A.; Yodh, A. G. *Nature* **2011**, *476*, 308−311.
(11) Deegan, R. D. *Phys. Rev. E* **2000**, *61*, 475−485.
(12) Stannard, A.; Martin, C. P.; Pauliac-Vaujour, E.; Moriarty, P.; Thiele, U. *J. Phys. Chem. C* **2008**, *112*, 15195−15203.
(13) Martin, C. P.; Blunt, M. O.; Moriarty, P. *Nano Lett.* **2004**, *4*, 2389−2392.
(14) Pauliac-Vaujour, E.; Moriarty, P. *J. Phys. Chem. C* **2007**, *111*, 16255−16260.
(15) Martin, C. P.; Blunt, M. O.; Pauliac-Vaujour, E.; Stannard, A.; Moriarty, P.; Vancea, I.; Thiele, U. *Phys. Rev. Lett.* **2007**, *99*, 116103.
(16) Pauliac-Vaujour, E.; Stannard, A.; Martin, C. P.; Blunt, M. O.; Notingher, I.; Moriarty, P.; Vancea, I.; Thiele, U. *Phys. Rev. Lett.* **2008**, *100*, 176102.
(17) Crivoi, A.; Duan, F. *Phys. Chem. Chem. Phys.* **2012**, *14*, 1449−1454.
(18) Vancea, I.; Thiele, U.; Pauliac-Vaujour, E.; Stannard, A.; Martin, C. P.; Blunt, M. O.; Moriarty, P. J. *Phys. Rev. E* **2008**, *78*, 041601.
(19) Lyushnin, A. V.; Golovin, A. A.; Pismen, L. M. *Phys. Rev. E* **2002**, *65*, 021602.
(20) Sztrum, C. G.; Hod, O.; Rabani, E. *J. Phys. Chem. B* **2005**, *109*, 6741−6747.
(21) Brutin, D.; Sobac, B.; Loquet, B.; Sampol, J. *J. Fluid Mech.* **2011**, *667*, 85−95.
(22) Yakhno, T. *J. Colloid Interface Sci.* **2008**, *318*, 225−230.
(23) Crivoi, A.; Duan, F. *J. Phys. Chem. C* **2013**, *117*, 7835−7843.
(24) Frastia, L.; Archer, A. J.; Thiele, U. *Phys. Rev. Lett.* **2011**, *106*, 077801.
(25) Archer, A. J.; Robbins, M. J.; Thiele, U. *J. Phys.: Condens. Matter* **2011**, *23*, 415102.
(26) Rabani, E.; Reichman, D. R.; Geissler, P. L.; Brus, L. E. *Nature* **2003**, *426*, 271−274.
(27) Kwek, D.; Crivoi, A.; Duan, F. *J. Chem. Eng. Data* **2010**, *55*, 5690−5696.
(28) Duan, F.; Kwek, D.; Crivoi, A. *Nanoscale Res. Lett.* **2011**, *6*, 248.
(29) Duan, F.; Wong, T. F.; Crivoi, A. *Nanoscale Res. Lett.* **2012**, *7*, 360.
(30) Sciortino, F.; Belloni, A.; Tartaglia, P. *Phys. Rev. E* **1995**, *52*, 4068−4079.
(31) Codling, E. A.; Plank, M. J.; Benhamou, S. *J. R. Soc., Interface* **2008**, *5*, 813−834.
(32) Okubo, A.; Levin, S. A. *Diffusion and Ecological Problems: Modern Perspectives*; Springer: Berlin, Germany, 2001; pp 143−150.
(33) Duan, F. *J. Phys. D: Appl. Phys.* **2009**, *42*, 102004.
(34) Duan, F.; Ward, C. A. *Langmuir* **2009**, *25*, 7424−7431.
(35) Xu, X.; Luo, J. *Appl. Phys. Lett.* **2007**, *91*, 124102.
(36) Thompson, I.; Duan, F.; Ward, C. A. *Phys. Rev. E* **2009**, *80*, 056308.